

Effects of the large distribution of CdS quantum dot sizes on the charge transfer interactions into TiO₂ nanotubes for photocatalytic hydrogen generation

This content has been downloaded from IOPscience. Please scroll down to see the full text.

2016 Nanotechnology 27 285401

(<http://iopscience.iop.org/0957-4484/27/28/285401>)

View [the table of contents for this issue](#), or go to the [journal homepage](#) for more

Download details:

IP Address: 200.128.60.24

This content was downloaded on 26/05/2017 at 13:00

Please note that [terms and conditions apply](#).

You may also be interested in:

[Optically modulated charge transfer in TiO₂-Au nano-complexes](#)

Zhufeng Shao, Zhaoshuo Tian, Junqi Pang et al.

[Mechanism of strong visible light photocatalysis by Ag₂O-nanoparticle-decorated monoclinic TiO₂\(B\) porous nanorods](#)

Kamal Kumar Paul, Ramesh Ghosh and P K Giri

[Titanium dioxide nanomaterials for photocatalysis](#)

Yan Liu, Zhe Li, Michael Green et al.

[Electron-transfer dependent photocatalytic hydrogen generation over cross-linked CdSe/TiO₂ type-II heterostructure](#)

Yubin Chen, Chi-Hung Chuang, Zhixiao Qin et al.

[Low-temperature liquid phase reduced TiO₂ nanotube arrays: synergy of morphology manipulation and oxygen vacancy doping for enhancement of field emission](#)

Xu-Qiang Zhang, Jian-Biao Chen, Cheng-Wei Wang et al.

[The fabrication and photoelectrocatalytic study of composite ZnSe/Au/TiO₂ nanotube films](#)

Guowei Zhang, Hui Miao, Yongbo Wang et al.

[Cu₂O/Ag co-deposited TiO₂ nanotube arrays film prepared by pulse reversing voltage and photocatalytic properties](#)

Qi Ding, Suiyuan Chen, Fanmin Shang et al.

[Recent progress in oxynitride photocatalysts for visible-light-driven water splitting](#)

Tsuyoshi Takata, Chengsi Pan and Kazunari Domen

Effects of the large distribution of CdS quantum dot sizes on the charge transfer interactions into TiO₂ nanotubes for photocatalytic hydrogen generation

Johan R González-Moya^{1,2}, Yunier Garcia-Basabe^{3,4},
Maria Luiza M Rocco³, Marcelo B Pereira⁵, Jefferson L Prival¹,
Luciano C Almeida¹, Carlos M Araújo⁶, Denis G F David⁷,
Antonio Ferreira da Silva⁷ and Giovanna Machado^{1,2}

¹ Universidade Federal de Pernambuco (UFPE), Recife, PE, Brazil

² Centro de Tecnologias Estratégicas do Nordeste (CETENE), Recife, PE, Brazil

³ Universidade Federal de Rio de Janeiro (UFRJ), Rio de Janeiro, RJ, Brazil

⁴ Universidade Federal da Integração Latino-Americana, UNILA, Foz do Iguaçu, PR, Brazil

⁵ Universidade Federal do Rio Grande do Sul (UFRGS), Instituto de Física, Porto Alegre, RS, Brazil

⁶ Uppsala University, Department of Physics and Astronomy, Uppsala, Sweden

⁷ Universidade Federal da Bahia (UFBA), Instituto de Física, Salvador, BA, Brazil

E-mail: jglez82@gmail.com and giovanna.machado@cetene.gov.br

Received 22 September 2015, revised 20 April 2016

Accepted for publication 3 May 2016

Published 2 June 2016




CrossMark

Abstract

Hydrogen fuels generated by water splitting using a photocatalyst and solar irradiation are currently gaining the strength to diversify the world energy matrix in a green way. CdS quantum dots have revealed a hydrogen generation improvement when added to TiO₂ materials under visible-light irradiation. In the present paper, we investigated the performance of TiO₂ nanotubes coupled with CdS quantum dots, by a molecular bifunctional linker, on photocatalytic hydrogen generation. TiO₂ nanotubes were obtained by anodization of Ti foil, followed by annealing to crystallize the nanotubes into the anatase phase. Afterwards, the samples were sensitized with CdS quantum dots via an *in situ* hydrothermal route using 3-mercaptopropionic acid as the capping agent. This sensitization technique permits high loading and uniform distribution of CdS quantum dots onto TiO₂ nanotubes. The XPS depth profile showed that CdS concentration remains almost unchanged (homogeneous), while the concentration relative to the sulfate anion decreases by more than 80% with respect to the initial value after ~100 nm in depth. The presence of sulfate anions is due to the oxidation of sulfide and occurs in greater proportion in the material surface. This protection for air oxidation inside the nanotubular matrix seemingly protected the CdS for photocorrosion in sacrificial solution leading to good stability properties proved by long duration, stable photocurrent measurements. The effect of the size and the distribution of sizes of CdS quantum dots attached to TiO₂ nanotubes on the photocatalytic hydrogen generation were investigated. The experimental results showed three different behaviors when the reaction time of CdS synthesis was increased in the sensitized samples, i.e. similar, deactivation and activation effects on the hydrogen production with regard to TiO₂ nanotubes. The deactivation effect was related to two populations of sizes of CdS, where the population with a shorter band gap acts as a trap for the electrons photogenerated by the population with a larger band gap. Electron transfer from CdS quantum dots to TiO₂ semiconductor nanotubes was proven by the results of UPS measurements combined with optical band gap measurements. This property facilitates an improvement of the visible-light

hydrogen evolution rate from zero, for TiO₂ nanotubes, to approximately 0.3 $\mu\text{mol cm}^{-2} \text{h}^{-1}$ for TiO₂ nanotubes sensitized with CdS quantum dots.

 Online supplementary data available from stacks.iop.org/NANO/27/285401/mmedia

Keywords: Brazilian MRS, TiO₂ nanotubes, quantum dots, photocatalysis, hydrogen generation, charge transfer

(Some figures may appear in colour only in the online journal)

1. Introduction

In recent years, the use of renewable and non-polluting energy has gained importance in the world due to the exhaustion of fossil fuels and the high levels of pollution generated from fossil fuel use. A promising form of clean and renewable energy is hydrogen produced by dissociation of water using solar energy and a photocatalyst material [1].

Since Fujishima and Honda [2] demonstrated photo-electrochemical water splitting using titanium dioxide (TiO₂) as the photoanode and Pt as the cathode, many types of materials based on either metal oxides or metal chalcogenides have been used as photocatalysts for H₂ production [3]. However, the most studied material is TiO₂ due to its good electronic, structural and morphological properties. TiO₂ has a strong oxidizing power, photo- and chemical-stability, non-toxic nature and low cost [4].

To achieve high yields in the photocatalytic reaction, a high surface area is desired. For this reason, the use of nanostructured materials, such as nanoparticles, nanowires, and nanotubes, have also received much attention in past two decades [4]. Among the several methods of preparing nanostructured TiO₂ [5], the synthesis of TiO₂ nanotubes (NTs) by anodization of metallic titanium has several advantages [6, 7], e.g., a simple synthetic procedure, supported photocatalyst obtainment, better charge carrier transport properties and a good cost–benefit relationship [8]. In addition, TiO₂ self-organized nanotubular arrays formed by the anodization process have better photocatalytic activity compared with TiO₂ nanoparticles or nanotubes synthesized by hydrothermal techniques [4, 8].

However, the principal drawback of TiO₂-based materials is its wide optical band gap of approximately 3.0 eV, meaning that only UV light is efficiently absorbed and the harvesting of the solar energy is limited (approximately 5% of the solar spectrum) [4]. To solve this problem, numerous studies have been performed to increase the photocatalytic activity of TiO₂ by applying modifications to harvest the visible light of the solar spectrum (~45%), e.g., TiO₂ doping with metallic and non-metallic elements, impregnation with noble metals, organic dyes, and quantum dots (QDs) sensitization, among others [9].

Particularly, some of the intrinsic properties of QDs have been advantageously explored in the sensitization of TiO₂ NTs to increase the photocatalytic activity of the NTs. As an example, QDs with tunable size and tunable band gap can be produced in the visible region with the ability to generate multiple excitons, presenting photostability, low cost and a

high molar extinction coefficient [10]. These characteristics help to increase the photocatalytic efficiency of systems of TiO₂ NTs sensitized with QDs.

There are several methods for the preparation of QDs and their impregnation in higher band gap semiconductor materials [11]. In general, these methods are separated into two major categories: *in situ* impregnation and fabrication with pre-synthesized colloidal QDs. Chemical bath deposition (CBD) and the successive ion layer adsorption and reaction (SILAR) are *in situ* methods that are well known and widely used. In the second category, the QDs are usually pre-synthesized and subsequently bound to TiO₂ materials using molecular linkers or physically adsorbed directly onto the material [10, 11].

Thioacid molecules are the most used as bifunctional linkers because of their great affinity to bind with both the TiO₂ and CdS via different parts of molecule [12]. In this context, some binders have been highlighted and we can mention the use of the meso-2,3-dimercaptosuccinic acid [13] and thiolactic acid [14, 15] to anchor semiconductor nanoparticles onto the surface of TiO₂ nanotubes, thereby improving the photocatalytic activity.

The inter-particle electron transfer is an important mechanism to improve the photocatalytic activity for these systems by visible-light harvesting [16]. For that reason, Watson *et al* [17] studied the dependence of electron transfer on the separation distance of CdS and TiO₂ particles by different lengths of molecular mercaptoalkanoic acids. They concluded that the electron injection yield decreases with increasing molecular chain length, and for a short bifunctional linker, such as 3-mercaptopropionic acid (MPA), the electron transfer is fast and efficient. Also, Qian *et al* [18] proved that the strong coupling between CdS and TiO₂ using the MPA bifunctional linker could promote the photocatalytic activity and also the stability of final photocatalyst.

Other studies have investigated the quantum dot size effect on inter-particle charge transfer [19, 20]. Kamat *et al* proved that the driving force for electron transfer is an energy difference of the conduction band of semiconductors and when the sizes of quantum dots become smaller the electron transfer to TiO₂ is faster and more efficient [19, 20].

Although coupled semiconductor systems are widely studied due to their interesting potential applications, not all of the phenomena involved in efficiency of photocatalysis are fully understood. Therefore, research on new routes of impregnation of TiO₂ nanotubes with different sizes of quantum dots and their characterization is required to better understand the mechanisms involved in photocatalytic

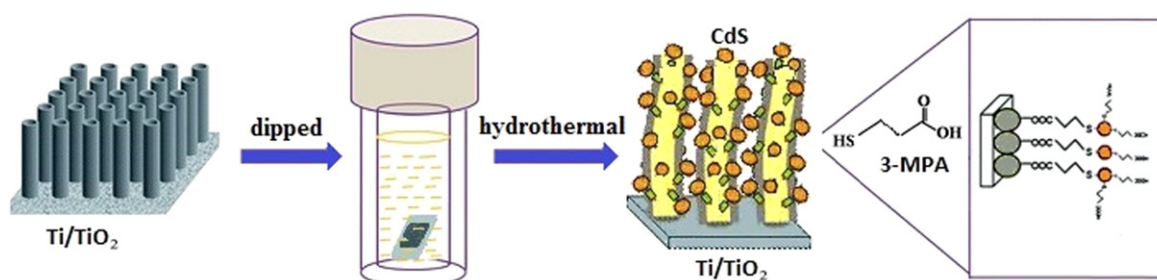


Figure 1. Schematic illustration for the synthesis of the TiO₂ nanotubes sensitized with CdS QDs using the *in situ* hydrothermal technique.

behavior and the dependence on different quantum dot size distributions.

Aiming to use visible light of the solar spectrum for hydrogen generation using a TiO₂-based photocatalyst, we prepared TiO₂ nanotubes using the anodization process, which, after annealing, were sensitized with different size distributions of CdS quantum dots coupled with MPA bifunctional linker. The samples were characterized by several techniques. UV-vis and visible-light hydrogen generation through photocatalytic water splitting were investigated, and the different behaviors of the photocatalytic activity using CdS QD sensitizers related to the sizes and distribution of sizes of QDs are discussed.

2. Experimental methods

2.1. Materials

The ethylene glycol 99% (ETG), NH₄F, CdCl₂ and 3-mercaptopropionic acid (MPA) were purchased from Sigma-Aldrich, acetone PA and titanium foil (98.6%) were from Synth, Na₂S · 9H₂O was from Alfa-Aesar, and Na₂SO₃ and NaOH were from Proquimios and Fmaia respectively. Solvents and reagents of analytical grade were used as received. Milli Q water was used in all the experiments.

2.2. Preparation of TiO₂ NTs by anodization

TiO₂ NTs were obtained by anodizing a 0.48 cm² of Ti foil (applied electrical potential 30 V with a Supplier AC Power Source) for 1 h in an ultrasonic bath. In this case, ETG solutions containing 0.7 wt.% NH₄F and 10 wt.% water were used [5, 21]. The time-dependent anodization current was recorded with a computer controlled Minipa ET-2076A multimeter.

Prior to anodization the Ti foil was cleaned ultrasonically in acetone for 10 min, rinsed with Milli Q water and dried under N₂ flux. The anodization was performed in a two-electrode configuration with titanium foil as the working electrode and platinum foil as the counter electrode.

After the anodization process, the samples were rinsed with water and dried in N₂ flux. In order to crystallize the TiO₂ nanotube arrays, the samples were annealed in a furnace at 400 °C for 3 h in atmospheric air.

2.3. Sensitization of TiO₂ nanotubes with CdS QDs

The TiO₂ nanotubes obtained by anodization were sensitized with CdS quantum dots using *in situ* the hydrothermal technique reported by Wang *et al* [22], with some modifications (figure 1).

More detailed preparations can be found in the supporting information stacks.iop.org/NANO/27/285401/mmedia along with a description of the characterization methods. TiO₂ nanotubes sensitized with CdS quantum dot samples will be referred to here as NTs_TiO₂ + CdS_{conc-time} and the derived colloidal CdS quantum dots as QDs_CdS_{conc-time} to facilitate the discussion. Here 'conc' is an initial concentration of CdCl₂ precursor on QDs synthesis and 'time' is a reaction time for a hydrothermal synthesis.

3. Results and discussions

3.1. Morphology and crystalline structure

TiO₂ NT arrays synthesized by electrochemical anodization of Ti foil were monitored in real time via the curve of current versus time. The current-time responses for different anodizations are very similar and exhibit a typical behavior for a formation of TiO₂ nanotubes via anodization in electrolytes containing fluoride ions [23], indicating the reproducibility of the process.

To crystallize the oxide film into the crystalline anatase phase, the amorphous as-anodized TiO₂ NT arrays were thermally annealed at 400 °C for 3 h in air. The anatase is a desirable phase due to its higher photocatalytic activity caused by a higher mobility of charge carriers versus that of amorphous TiO₂ [4, 24].

The XRD patterns (figure S1, supporting information) confirm the crystallization into anatase phase. The diffractogram of the as-anodized TiO₂ NT sample shows a typical behavior of an amorphous material but also shows diffraction peaks corresponding to the hexagonal metallic titanium (JCPDS file No 8927-62) used to grow the nanotubes during the anodizing process. After the annealing process, Bragg reflections in 25.4°, 48.2°, 53.9° and 55.1° appear in the sample. These peaks correspond to the crystal planes (101), (200), (105) and (211) of the TiO₂ anatase phase (JCPDS file No 8412-86).

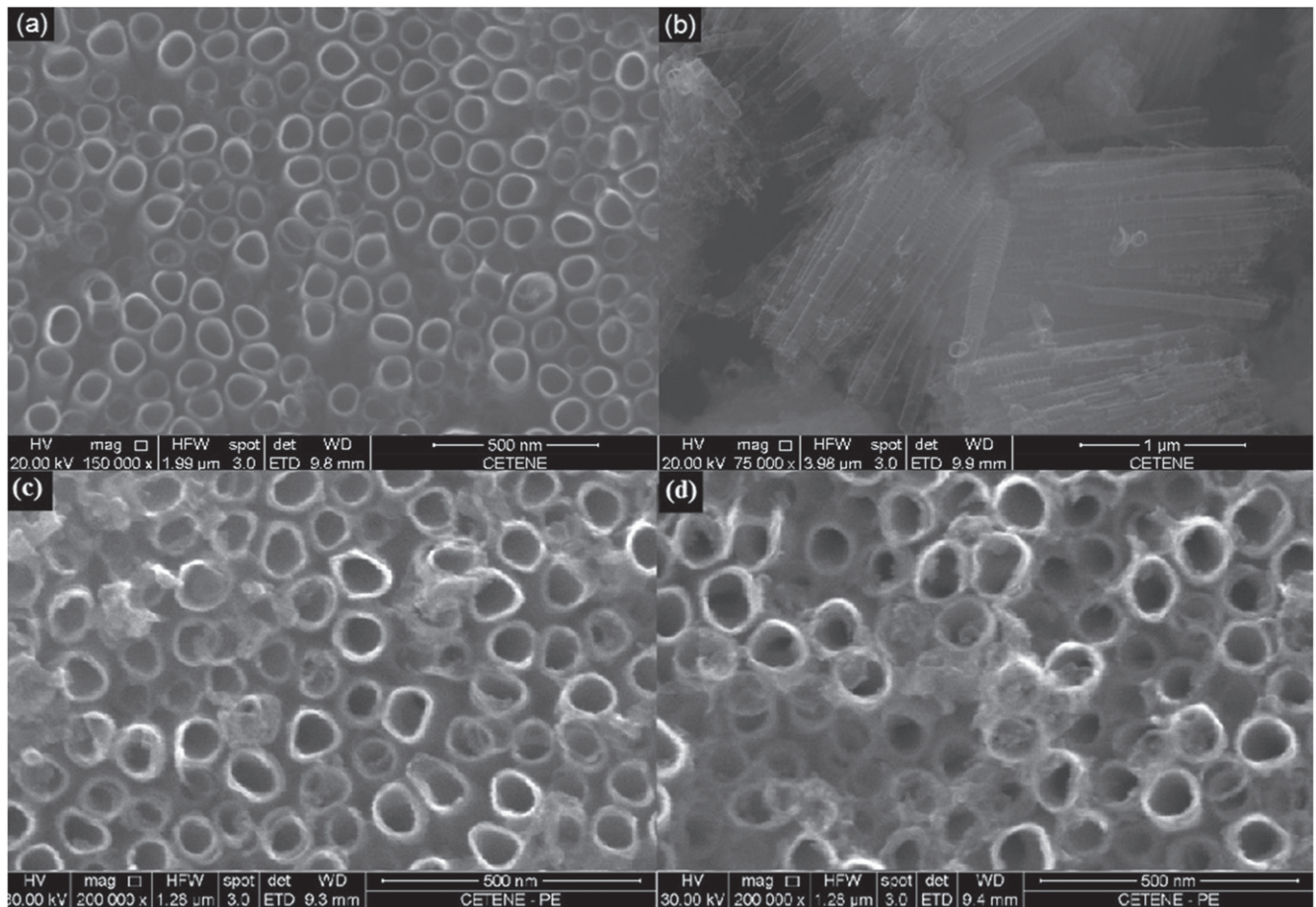


Figure 2. SEM images of top view (a) and side view (b) of TiO_2 nanotubes. Top view of a sensitized samples $\text{NTs_TiO}_2 + \text{CdS}_{5\text{mM-}120 \text{ min}}$ (c) and $\text{NTs_TiO}_2 + \text{CdS}_{10\text{mM-}120 \text{ min}}$ (d).

The morphology of the obtained TiO_2 NTs was evaluated by scanning electron microscopy (SEM). Figures 2(a) and (b) show the SEM images of typical TiO_2 NTs obtained by the anodization process. For the TiO_2 NTs, the average value of internal diameter is 68.0 ± 8.0 nm and the average wall thickness is 10.7 ± 2.0 nm, estimated by measuring more than 200 nanotubes using ImageJ software. The average length of NTs is slightly above $2 \mu\text{m}$, as obtained from the side view SEM images.

After the sensitization of TiO_2 NTs with CdS QDs via the *in situ* hydrothermal route, no significant changes in nanotubular morphology were observed. For the samples synthesized with 1 mM of CdCl_2 precursor, the CdS QDs were not observable directly on the SEM images because the size of the nanoparticles is smaller than the resolution of the scanning electron microscope. Nonetheless, for more concentrated samples (5 mM and 10 mM of CdCl_2 precursor), some particle agglomeration was observed on the top surface of TiO_2 nanotubes (figures 2(c) and (d)). The agglomerations of CdS QDs on the TiO_2 nanotube arrays are due to the higher concentration of QDs for these samples.

To better identify the presence of the CdS QDs in the materials, EDS mapping for Cd and S elements was performed (figure S2, supporting information). This figure identifies the uniform presence of the elements throughout the

TiO_2 nanotubular matrix, confirming that the distribution of CdS on the TiO_2 NTs is homogeneous, at least in the two dimensions of the top surface studied so far.

TEM images of the $\text{NTs_TiO}_2 + \text{CdS}_{10\text{mM-}120 \text{ min}}$ sample were also taken (figure 3) to explore the interaction between the TiO_2 and CdS semiconductors. In the TEM image (figure 3(a)), we can observe the presence of CdS nanoparticles attached to the TiO_2 nanotubes. This observation is corroborated by the HRTEM image (figure 3(b)), where the TiO_2 and CdS semiconductors are closely related. In the HRTEM image the spacings of the visible lattice fringes were measured to be 0.29 nm and 0.24 nm and is in agreement with the interplanar distances of the (102) crystallographic planes for anatase TiO_2 (JCPDS file No 8412-86) and the (102) crystallographic planes for hexagonal CdS (JCPDS file No 7723-06), respectively.

3.2. Chemical surface

To determine surface chemical composition and oxidation state of CdS on the TiO_2 samples, XPS measurements were performed. The XPS survey spectra of the TiO_2 nanotubes and the CdS QD sensitized samples (figure S3, supporting information) indicate that Ti, O and C are present on both samples; in addition to the above elements, Cd and S are also

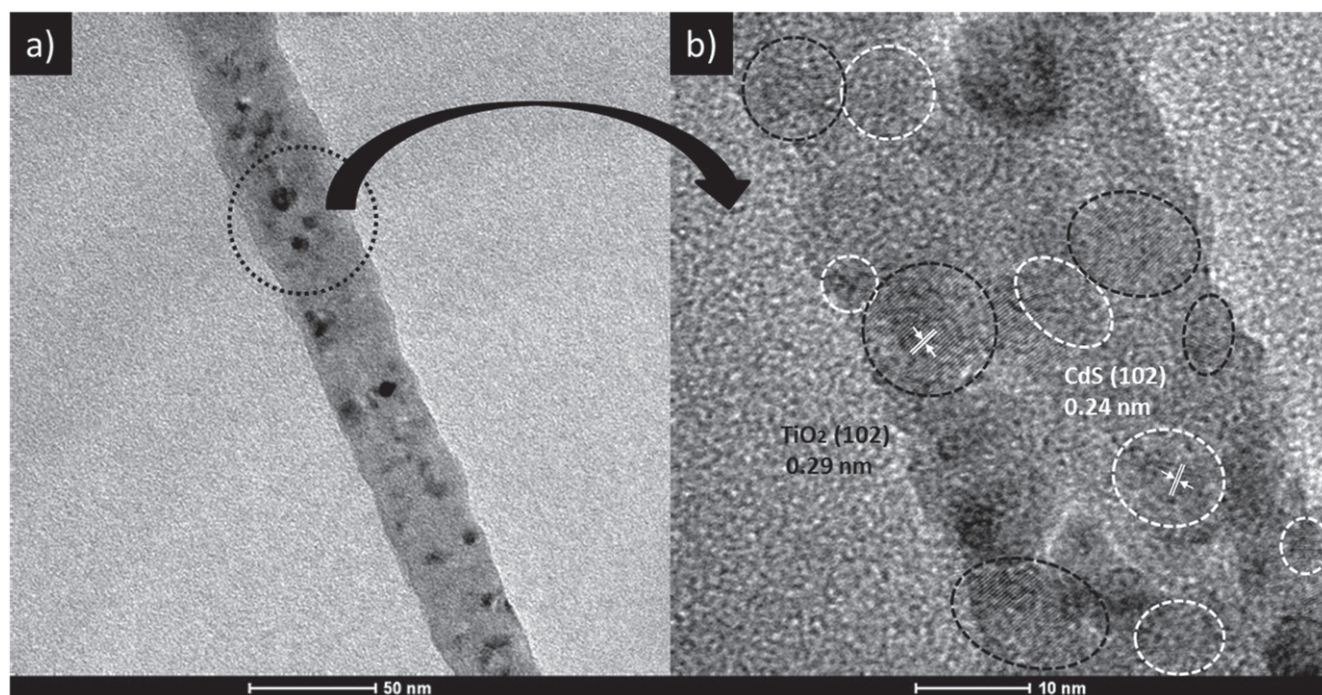


Figure 3. TEM image (a) and HRTEM image (b) of NTs_{TiO₂} + CdS_{10mM_120 min} sample.

Table 1. Elemental chemical analysis for the XPS survey (atomic %).

Sample	Ti	O	C	Cd	S	Cd/Ti	S/Cd
NTs _{TiO₂}	16.9	49.5	33.6	—	—	—	—
NTs _{TiO₂} + CdS _{10mM_120 min}	14.1	47	32.0	2.93	3.97	0.21	1.35

present in NTs_{TiO₂} + CdS_{10mM_120 min}. Carbon and some contribution of oxygen probably stemmed from the air and/or impurity of the molecules containing these elements during the synthesis procedure.

The elemental chemical compositions obtained from the survey XPS spectra are reported in table 1. For the sample NTs_{TiO₂} + CdS_{10mM_120 min}, the Cd/Ti atomic ratio is 0.21, i.e., the coverage of the CdS QDs is approximately 21% with respect to titanium on the TiO₂ nanotube surface [25]. The S/Cd atomic ratio is 1.35; this means that the CdS QDs we obtained are slightly S rich, and this result is expected because of the use of MPA as a stabilizer.

The high-resolution XPS spectra for each core level were also collected. In the case of the high-resolution XPS spectra of Ti 2p (figure S4, supporting information), no significant difference was observed between the NTs_{TiO₂} and NTs_{TiO₂} + CdS_{10mM_120 min} samples. Both samples have a binding energy for Ti 2p_{3/2} of 459.3 eV, which is associated with Ti (IV) on the titanium dioxide [26, 27]. The binding energy of 530.4 eV for the most intense O 1s peak (figure S5, supporting information) also indicates that both samples are comprised of titanium dioxide compounds.

The O 1s XPS spectrum is composed of chemically distinct oxygen contributions [27], due primarily to the oxygen related to TiO₂ and the oxygen of different groups of organic molecules used at different stages of the synthesis

and/or impurities. The O 1s signals for the TiO₂ NTs sensitized with CdS QDs show a more pronounced shoulder at higher binding energies (figure S5(b), supporting information) due to the contribution of the 534.2 eV peak, which is not present in the spectra of the TiO₂ nanotube sample (figure S5(a), supporting information). This additional peak may be associated with MPA due to the oxygen atoms in the carboxyl group [28]. The MPA is used during the sensitization of TiO₂ NTs with CdS QDs to stabilize the nanoparticles; in contrast, no MPA is present in the TiO₂ NT sample.

The high-resolution XPS spectra of the Cd 3d core level for the NTs_{TiO₂} + CdS_{10mM_120 min} sample (figure S6, supporting information), is characterized by Cd 3d_{5/2} and Cd 3d_{3/2} peaks centered at 405.9 and 412.6 eV, respectively, with a spin-orbit separation of 6.7 eV; these peaks can be assigned to the CdS nanoparticles [29, 30].

In addition, figure 4(a) shows the high-resolution XPS spectra of the S 2p core level for the same sample. The S 2p spectrum is formed by four peaks, which can be divided into two S chemically distinct environments. The two higher intensity peaks at 162.5 and 163.7 eV are the S 2p_{3/2} and S 2p_{1/2} spin-orbit components of S²⁻, respectively, with a difference in binding energy of 1.2 eV and an intensity ratio of approximately 2:1, showing an excellent agreement with the S²⁻ signal previously reported for CdS nanoparticles [30]. The lower intensity peaks at higher binding energies of 169.4

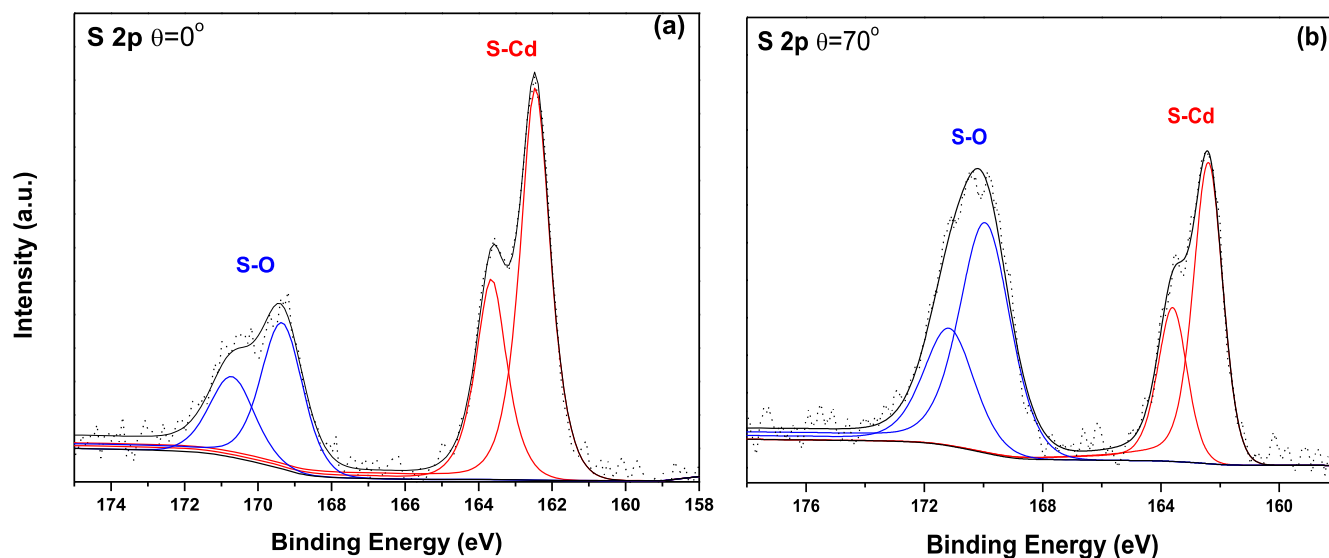


Figure 4. High-resolution angle resolved XPS spectra of S 2p core levels for NTs_TiO₂ + CdS_{10mM-120 min} sample. $\theta = 0^\circ$ (a) and $\theta = 70^\circ$ (b) with respect to the surface normal.

and 170.7 eV correspond to the S 2p_{3/2} and S 2p_{1/2} spin-orbit components of the sulfate species, respectively [30]. This result suggests that the CdS QDs presented in TiO₂ NT films are partially oxidized.

High-resolution XPS spectra of S 2p collected at a grazing angle (figure 4(b)) show a strong increase of relative S-O/S-Cd peaks compared with the normal incidence S 2p XPS spectra (figure 4(a)). These results prove that the partial oxidation of CdS QDs has a surface character.

This surface oxidation is expected because the oxidation process will be more efficient on the top of TiO₂ NT surface where contact with air is greater and easier than on the inner surface of the nanotubes, where contact with oxygen is controlled by diffusion within the small nanotubes (~10 nm of mouth diameter) and some blocking because of CdS QD aggregation in the top surface, as discussed above for the concentrated samples.

The surface character of the partial oxidation of CdS QDs is also corroborated by XPS depth profile measurements (figure 5), where the S-O contribution decreases with the nanotube's depth to a minimum level after a depth of approximately 100 nm. This result shows that the oxidation of CdS occurs superficially and the parts of the sample that are deeper than 100 nm will be protected from air oxidation, perhaps due to CdS QD agglomeration in the surface, blocking the open channel of TiO₂ nanotubes.

The XPS depth profile also shows that the Cd and S total content remains almost unchanged with nanotube depth, within the experimental uncertainty. These results are evidence of the vertical homogeneous distribution of the CdS QDs onto the TiO₂ NT arrays, which, combined with the previous result obtained by EDS mapping, allows us to conclude that the CdS QDs have a homogeneous distribution among the TiO₂ NT arrays in three dimensions.

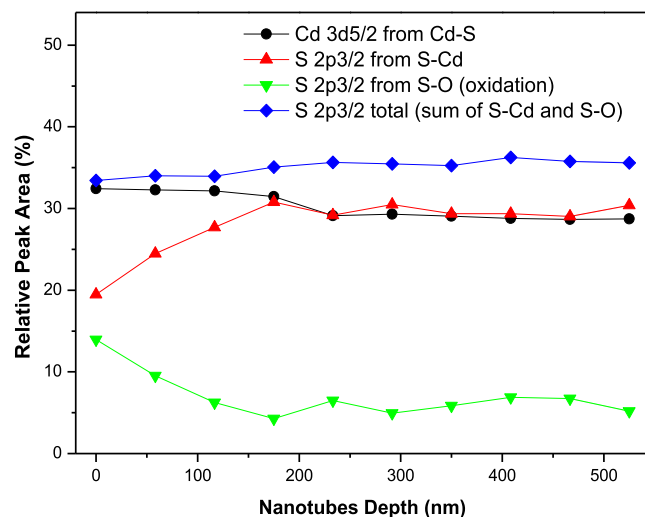


Figure 5. XPS depth profile of Cd 3d_{5/2} and S 2p_{3/2} for the NTs_TiO₂ + CdS_{10mM-120 min} sample. (0 depth is the top surface of samples).

3.3. Optical absorption properties

In the sensitization process using the *in situ* hydrothermal technique, a capping agent (MPA) has a key role in the synthesis: serving as a stabilizer for the QDs CdS (the thiol group of MPA has strong affinity for Cd²⁺ cations present in the CdS nanoparticles surface) [31], and also functioning as a linker to the TiO₂ NT surface through its carboxyl group because TiO₂ has a strong affinity for the carboxylate group present in these HS-R-COOH types of ligands [18, 32]. Another advantage of using MPA is related to better surface passivation of QDs, leading to an increase in carrier mobility and decrease in charge recombination [33, 34].

During the *in situ* hydrothermal reaction process, one part of the CdS precursors will diffuse into the nanotubular

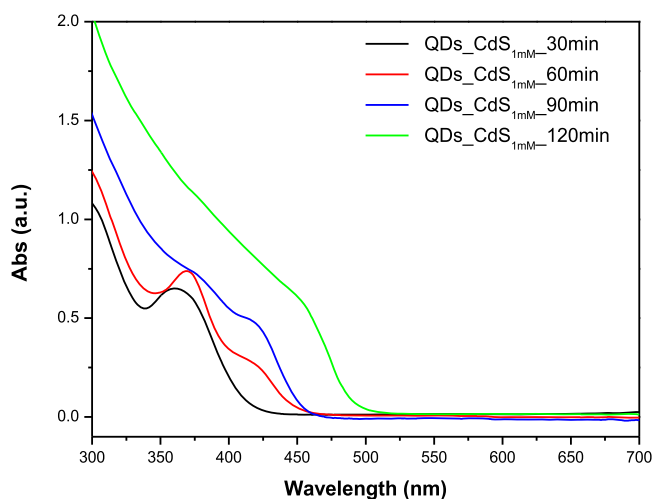


Figure 6. UV-vis absorption spectra of colloidal CdS QDs.

structure with better efficiency, due to their ion-scale dimensions [12], reacting and bonding chemically on the TiO₂ surfaces through the carboxylate anchoring group of MPA to obtain the sensitized samples [18]. Simultaneously, the other parts of the precursors will form colloidal CdS quantum dots stabilized by MPA via the general hydrothermal synthesis [31].

The UV-vis spectra of the derived colloidal CdS QDs were obtained to roughly estimate the size and distribution of sizes of the CdS QDs attached to the TiO₂ NTs arrays because, according to the literature [12], the QDs grown in confined TiO₂ mesoporous structures are slightly smaller than those grown in the free solution due to diffusion limits.

Figure 6 shows the collected UV-vis spectra of CdS QD colloidal suspensions obtained from 1 mM Cd²⁺ precursors at 180 °C for different reaction times. One can observe that all spectra have an absorption edge below 513 nm, which is the value for bulk CdS, demonstrating that the obtained CdS QDs exhibit quantum confinement [35, 36].

The QDs_CdS_{1mM_30 min} colloid showed a well-defined and narrow excitonic peak at approximately 360 nm, suggesting the formation of monodisperse nanoparticles of CdS. Similar results have been reported for other semiconductor QD systems [37, 38].

An increase in the reaction time leads to a gradual red shift of the absorption peak, indicating an increase in the average diameter of the nanoparticles obtained [37]. For colloids obtained at 60 and 90 min of hydrothermal reaction, the presence of a second shoulder may be explained by two populations of nanoparticles present in a bimodal distribution of sizes.

For the QDs_CdS_{1mM_120 min} colloid, a broad excitonic peak at approximately 454 nm was observed, indicating a larger size distribution for the CdS QDs obtained at these conditions. This also verified that a longer heating time (150 min) led to a fine yellow precipitate of CdS bulk. Therefore, for reaction times above 150 min, the amount of MPA used was not sufficient to stabilize the nanoparticle

Table 2. Band gap and average size of CdS QDs.

Sample	λ_{\max} (± 1 nm)	QDs size (± 0.2 nm)	Band Gap (± 0.1 eV)
QDs_CdS _{1mM_30 min}	361	2.3	3.1
QDs_CdS _{1mM_60 min}	369	2.5	3.1
	421	4.1	2.8
QDs_CdS _{1mM_90 min}	380	2.8	2.9
	421	4.1	2.8
QDs_CdS _{1mM_120 min}	454	5.4	2.6
QDs_CdS _{5mM_60 min}	376	2.7	3.1
QDs_CdS _{10mM_60 min}	371	2.6	3.0
QDs_CdS _{5mM_120 min}	439	4.8	2.6
QDs_CdS _{10mM_120 min}	458	5.6	2.5

system, leading to the formation of a precipitate of CdS bulk. These samples were not used for further investigation.

The UV-vis spectra of colloidal suspensions of CdS QDs (180 °C, 60 min and 120 min) with different concentrations of the precursors (1 mM, 5 mM and 10 mM) were also studied (figure S7 and S8 in the supporting information). The absorption patterns for these suspensions were similar and presented an increase of absorbance when the concentration of the precursors was higher. Therefore, the concentration of CdS nanoparticles in the colloid increased, but the size distribution of the CdS QDs was quite similar. These results suggest that the concentration of the precursors in the range studied did not greatly affect the mechanism of CdS QD crystal growth.

The overall results show that the CdS QDs synthesized with different hydrothermal conditions presented a varied range of sizes (~2.31 to 5.63 nm), allowing for a variation of the reaction time to tune the sizes and, thus, their optical properties, i.e., tuning the absorption over the spectral range from UV to visible light (~300 to 500 nm).

For the different CdS QD colloids, the average size of the nanoparticles was estimated using an empirical correlation [39], which describes a good approximation for the dependence of the UV-vis maximum absorption with the size of the CdS QDs [40]. The optical band gaps were deduced from the Tauc plot of $(\alpha h\nu)^2$ versus photon energy for a CdS direct semiconductor [41]; the values of the QD sizes and optical band gaps are presented in table 2. In the case of samples QDs_CdS_{1mM_60 min} and QDs_CdS_{1mM_90 min}, the values related to the two absorption peaks are reported, suggesting a bimodal size distribution with centers at the reported sizes. The calculated sizes of CdS QDs are in agreement with the sizes estimated by TEM images within experimental error, given the poor statistics of particles measured in the images.

The UV-vis absorption spectra of TiO₂ NT sensitized samples were obtained by diffuse reflectance spectroscopy using a Kubelka-Munk function [42]. Figure 7 shows the UV-vis absorption spectra for the TiO₂ NTs after annealing

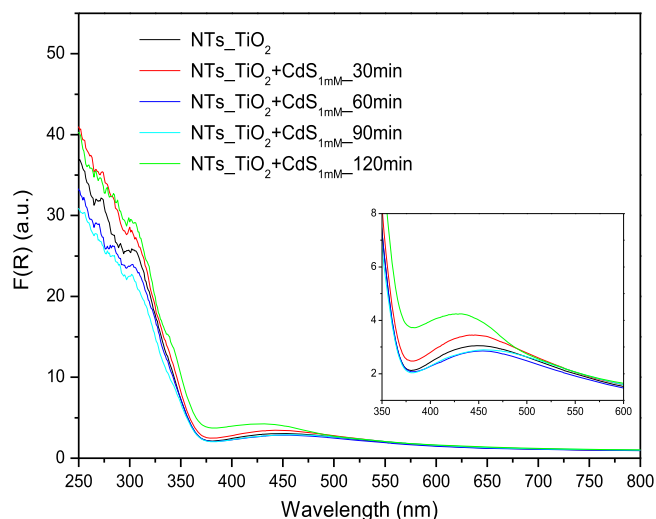


Figure 7. UV-vis spectra of TiO₂ NTs sensitized with CdS QDs at different conditions. Inset (magnified view of 350–600 nm region).

and the TiO₂ NTs sensitized with CdS QDs obtained by *in situ* hydrothermal techniques with different reaction times and a fixed concentration of the precursors (1 mM Cd²⁺). All spectra are similar and present a strong absorption in the ultraviolet region due to the absorption characteristic of anatase TiO₂ [43]. However, some sensitized samples exhibit slightly greater absorption in the visible region (400–500 nm) (Inset, figure 6) compared with the absorption of the NTs_TiO₂ sample due to the presence of the CdS QDs with smaller band gaps [44]. For NTs_TiO₂ + CdS_{1mM_60 min} and NTs_TiO₂ + CdS_{1mM_90 min} samples, the two CdS absorption peaks were not observed, similar to CdS colloids, because the concentration of CdS is lower than TiO₂ and the peak around 370 nm could be covered by the more intense TiO₂ absorption.

The band gap (E_g) of TiO₂ was estimated around 3.2 eV, using a Tauc plot of $(F(R)h\nu)^{1/2}$ versus photon energy, which is typically used to characterize an indirect band gap semiconductor [41, 42]. This value is very similar within the experimental error to that reported in the literature for the anatase phase of TiO₂ [43].

The estimated band gap for the CdS QDs attached to TiO₂ NTs for the different reaction times (30, 60 and 90 min) are in the ultraviolet region, so there would be no effective sensitization by absorption in the visible range for these samples. The more concentrated sensitized samples (5 mM and 10 mM) with 60 min of hydrothermal synthesis exhibit a low absorption in the visible region, similar to the NTs_TiO₂ sample (figure S9(a), supporting information). These results reinforce the hypothesis that, for these hydrothermal conditions, the sensitization is not efficient because an increase in the concentration of CdS QDs does not increase their absorption in the visible region.

On the other hand, for the samples obtained with 120 min of hydrothermal synthesis a significant increase of absorption in the visible region with increasing concentration of the precursors was observed (1, 5, 10 mM of Cd²⁺) (figure S9(b), supporting information). The above results allow us to

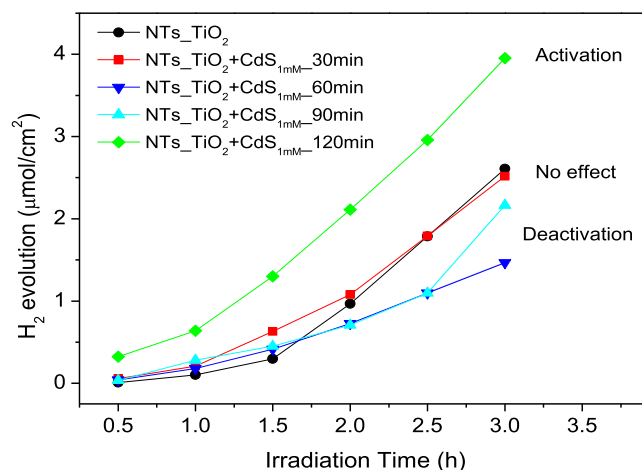


Figure 8. Hydrogen evolution with UV-vis irradiation time for TiO₂ NTs sensitized with CdS QDs (1 mM CdCl₂ precursor).

conclude that, for 120 min of reaction time, a real sensitization of TiO₂ NTs by CdS QDs occurs. Furthermore, these samples showed better photocatalytic activity, which will be discussed below.

3.4. Photocatalytic activity and photocurrent response.

The photocatalytic activity of the samples was evaluated for hydrogen production via the water splitting reaction using a sacrificial agent S²⁻/SO₃²⁻ 0.1 M in aqueous solution (pH = 12.5). This mixture acts as hole scavenger to improve the efficiency in the photocatalytic system and it can reduce the CdS photocorrosion [45, 46]. Figure 8 shows the hydrogen evolution with UV-vis irradiation time for TiO₂ NTs sensitized with CdS QDs (1 mM CdCl₂) at different hydrothermal conditions.

The apparent autocatalytic behavior observed in all the experiments is due to the fact that, before we can detect the hydrogen produced by photocatalysis in the headspace of the reactor, the sacrificial solution must first reach a gas saturation. During this time we observe an apparently smaller hydrogen evolution. The UV irradiation may also help to clean the samples from some impurities adsorbed on the surface, increasing the hydrogen production after approximately one hour of irradiation.

In figure 8, the TiO₂ NTs sensitized with CdS QD samples are observed to exhibit three different behaviors regarding the TiO₂ NTs photocatalyst. In the first case, the sample NTs_TiO₂ + CdS_{1mM_30 min} produces practically the same content of hydrogen as that with TiO₂ NTs, resulting in practically zero effect on the photocatalytic activity of TiO₂ NT materials.

The second behavior is a negative effect: in the samples NTs_TiO₂ + CdS_{1mM_60 min} and NTs_TiO₂ + CdS_{1mM_90 min}, the H₂ production decreases, so the CdS QDs added at these conditions have a deactivation effect. The activation effect is observed in the NTs_TiO₂ + CdS_{1mM_120 min} sample where the H₂ production increases compared to TiO₂ NTs.

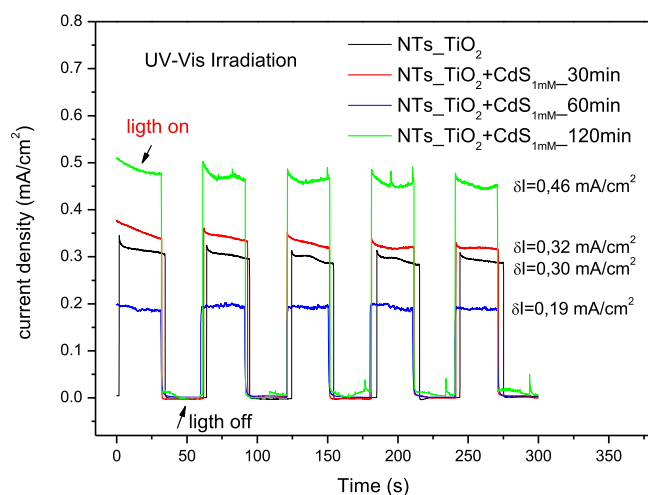


Figure 9. Photocurrent response of TiO₂ NT sensitized samples under UV-vis irradiation with on/off cycles at applied voltage of 0.0 V versus Ag/AgCl.

To better study these effects, a representative sample in each of the different behaviors was taken as the photoanode and the on/off photocurrent cycles were measured in a three-electrode photoelectrochemical cell. Figure 9 shows the photocurrent response using the same S²⁻/SO₃²⁻ 0.1 M electrolyte and UV-vis irradiation for different samples. We also measured the on/off photocurrent cycles for visible irradiation ($\lambda > 420$ nm) with the same conditions for each sample. The photocurrent response, due mainly to ultraviolet irradiation, was calculated as a difference between two experimental results obtained above. The overall results are shown in table 3.

The results of photocurrent response observed in figure 9 agreed with the results obtained for H₂ evolution in photocatalysis experiments (figure 8). This is expected, because the H₂ evolution is proportional to photocurrent response, and both are related to the quantity of electrons generated by the absorptions of photons from the UV-vis light source [47].

The different behaviors can be explained by the absorption properties of CdS QDs and their ability to transfer electrons to the conduction band of TiO₂ to increase its photocatalytic activity. The driving force for this electron transfer is a difference of energy between the conduction bands of electron donor CdS QDs and electron acceptor TiO₂ semiconductors [48, 49].

Taking the estimated band gap for colloidal CdS QDs as a reference (table 2), we consider that the band gap of CdS QDs present in NTs_TiO₂ + CdS_{1mM_30 min} (~3.1 eV) is practically the same as TiO₂ (~3.2 eV). Thus, CdS QDs absorb the same UV wavelengths as TiO₂, but rapidly transfer the photogenerated electrons to TiO₂ semiconductors, resulting in no influence on its photocatalytic activity. The overall process is shown schematically in figure 10(a). All diagrams are based on the band positions for TiO₂ and CdS systems [50], and in our band gap estimation for each sample.

Then, under our experimental conditions, for 30 min of *in situ* hydrothermal reaction, the desired sensitization is not

achieved due to the small size and the large band gap of the CdS QDs impregnated onto the TiO₂ NT material.

In the case of the NTs_TiO₂ + CdS_{1mM_60 min}, two size populations are verified (table 2). The one with a large band gap has a similar value (~3.1 eV) to the TiO₂, and we expected no behavioral effect in the ultraviolet region as observed for NTs_TiO₂ + CdS_{1mM_30 min} sample. In contrast to what we expected, the significant photocurrent reduction in the ultraviolet region (table 3) compared to NTs_TiO₂ was observed for this sample. Despite a slight increase of photocurrent in the visible region (table 3), the large reduction of photocurrent in the ultraviolet region is responsible for a reduction of overall UV-vis photocatalytic activity for this sample.

The two size populations present in the NTs_TiO₂ + CdS_{1mM_60 min} sample seem to be responsible for decreasing the photocatalytic activity of TiO₂ NTs. The CdS QDs with a large band gap absorb approximately the same UV light wavelengths as TiO₂, but these particles can transfer the photogenerated electrons in two thermodynamically possible ways: to the TiO₂ NTs, or to the CdS nanoparticles with a short band gap, a large part of which function as a trap for these electrons, leading to recombination or other processes instead of the desired H₂ generation.

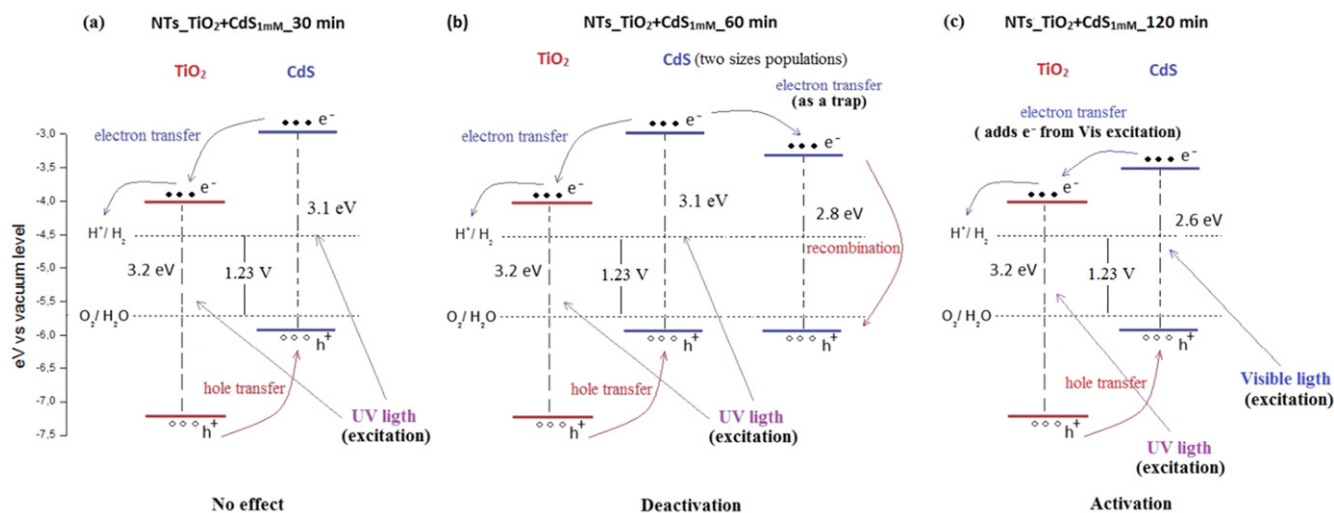
The overall process is shown schematically in figure 10(b). Both semiconductors will absorb approximately the same UV light wavelengths, leading to a competition regarding which species absorbs the photons that could be used to generate charges for the water splitting reaction. Part of this charge is trapped for a CdS with a shorter band gap and used in other processes or recombination, which results in a lower H₂ production.

In general the two sizes or greater population of quantum dots are a good thing for the sensitization of TiO₂ if synthesized in an ordered way (from larger to smaller QD sizes with regard to the TiO₂ surface) like in quantum dot rainbow solar cell approach studies [51]. This approach permits a high absorption over the visible spectrum and an effective electron transfer from smaller to larger QDs and finally to the TiO₂, like a cascade, because the conduction bands are properly positioned to transfer the electrons by the energy driving force [51].

In contrast, under our experimental conditions for 60 and 90 min of *in situ* hydrothermal reaction, the CdS QDs impregnated onto TiO₂ NTs material are of two size populations but randomly positioned regarding the TiO₂ NTs. The part of the sample where the conduction bands are properly positioned leads to a slight increase in the photocatalytic activity by visible-light absorption (table 3). On the other hand, the part of the sample where the conduction bands are positioned, as presented in figure 10(b), further diminish the photocatalytic activity from ultraviolet light absorption (table 3). The overall results for these samples are a deactivation effect on the photocatalytic activity of TiO₂ NTs, and to the our best of knowledge, this is the first time such a deactivation effect of the two sizes of CdS QDs onto a TiO₂-based photocatalyst has been reported in the literature.

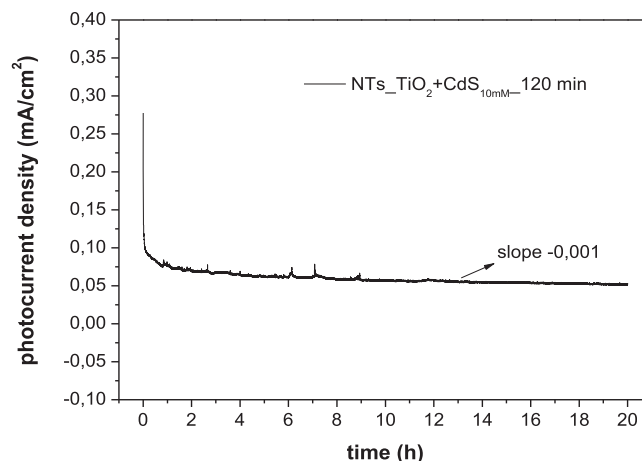
Table 3. Photocurrent response of TiO₂ NT sensitized samples. The δI (UV) column was calculated as a difference of two experimental data sets (δI (UV-vis)– δI (Vis)).

Sample	δI (UV-vis) experimental (mA cm ⁻²)	δI (Vis) experimental (mA cm ⁻²)	δI (UV) calculated (mA cm ⁻²)
NTs_TiO ₂	0.3	0.009	0.29
NTs_TiO ₂ + CdS _{1mM-30 min}	0.32 (~)	0.023	0.30
NTs_TiO ₂ + CdS _{1mM-60 min}	0.19 (-37%)	0.038	0.15
NTs_TiO ₂ + CdS _{1mM-120 min}	0.46 (+53%)	0.14	0.32

**Figure 10.** Schematic UV-vis excitations and charge transfer process for different behaviors as a photocatalyst. No effect (a), deactivation (b) and activation (c) proposed models.

A similar deactivation process was proven in the literature for the ternary TiO₂/CdSe/CdS photoanode [52], where electrons photogenerated by CdSe absorption could transfer to TiO₂ or to CdS; two possible ways due to the more negative CdSe conduction band. On the other hand, when the system is obtained in the other way (TiO₂/CdS/CdSe) the electron transfer was promoted like a cascade, improving the photocurrent response [52].

Finally, the NTs_TiO₂ + CdS_{1mM-120 min} sample produces approximately 51% more hydrogen via water splitting than TiO₂ NTs for the first 3 h of UV-vis irradiation (figure 8), and the photocurrent response is also 53% greater than TiO₂ NTs (table 3) in the same conditions. The activation behavior of this sample is explained by the significant absorption increase in the visible range with respect to TiO₂ NT material (figure 6, inset). The sensitizer (CdS QDs) absorbs more photons in the visible region to generate electrons, which are then quickly transferred to the TiO₂ and are available to the water splitting reaction [48, 49]. This additional absorption increases the photocatalytic activity of TiO₂ NT-based materials. In fact, the photocurrent response from visible-light absorption increases more than 15-fold compared to TiO₂ NTs (table 3) for a NTs_TiO₂ + CdS_{1mM-120 min} sample, proving the effective sensitization through visible-light absorption. The overall excitation and charge transfer process are presented schematically in figure 10(c) for a better visualization. From our experimental data, we found that

**Figure 11.** Photocurrent plots at 0 V versus Ag/AgCl and 1 Sun visible-light (>420 nm) irradiation.

better hydrogen production occurs for samples obtained via *in situ* hydrothermal techniques with 120 min of reaction time.

3.5. Stability study

To test the stability of our photocatalysts the NTs_TiO₂ + CdS_{10mM-120 min} sample was taken as the photoanode and long duration photocurrent measurements was made [53].

Figure 11 shows the photocurrents over 20 h using the same $\text{S}^{2-}/\text{SO}_3^{2-}$ 0.1 M electrolyte and visible-light (>420 nm) irradiation. The initial stabilized photocurrent (1 h) was compared with the final photocurrent (20 h) to calculate the photocurrent decay [54]. The calculated photocurrent decay was 1.3% for each hour on average, showing good stability properties in the sacrificial electrolyte.

These good stability properties are related to the use of MPA as a covalent linker between the TiO_2 and CdS semiconductors, leading to better anchoring properties if compared with samples without bifunctional covalent linkers in literature [18]. The stability may also relate to ordered nanotubular arrays that minimized the photocorrosion of CdS attached inside the TiO_2 NTs, in a similar way to how air oxidation is minimized, as explained above for depth profile XPS results.

Assuming that all generated photocurrent is used in water reduction for H_2 gas evolution, the hydrogen generation rate (v_{H_2}) can be calculated by the photocurrent from the following equation [47]: $v_{\text{H}_2} = 3600 * j_{\text{ph}} / 2F$, where j_{ph} is a photocurrent density (mA cm^{-2}) at the measurement applied bias and F is the faradic constant. Taking the average j_{ph} value (0.058 mA cm^{-2}) for an $\text{NTs}_{\text{TiO}_2} + \text{CdS}_{10\text{mM}-120 \text{ min}}$ sample, we estimated a hydrogen generation rate (v_{H_2}) of $1.08 \mu\text{mol cm}^{-2} \text{ h}^{-1}$.

The hydrogen generation rate was also estimated for the direct hydrogen quantifying method as explained in the supporting information and results in an evolution rate of $0.3 \mu\text{mol cm}^{-2} \text{ h}^{-1}$. The big difference between the hydrogen generation rates obtained for the two different methods is related to assuming 100% faradic efficiency for the calculated photocurrent measurements and also the use of a potential bias during the experiments. Both approaches overestimated the H_2 evolution rate for photoelectrochemical experiments if compared with photocatalytic methods [55].

3.6. Electron transfer study by UPS techniques

In order to prove the charge transfer between the electron donor CdS QDs and the electron acceptor TiO_2 NTs in the sensitized systems, ultraviolet photoelectron spectroscopy (UPS) experiments were performed. Figure S10 in the supporting information show the UPS spectra for the $\text{NTs}_{\text{TiO}_2}$ and $\text{NTs}_{\text{TiO}_2} + \text{CdS}_{10\text{mM}-120 \text{ min}}$ samples. The spectra were divided into lower and higher binding energy regions to investigate the effect of CdS QD sensitizers on the valence band and the effective work function (Φ) of the TiO_2 NTs materials, respectively.

The valence band maxima (VB_M) of 2.40 and 2.36 eV below the Fermi level were obtained for $\text{NTs}_{\text{TiO}_2}$ and $\text{NTs}_{\text{TiO}_2} + \text{CdS}_{10\text{mM}-120 \text{ min}}$ samples, respectively [56]. Furthermore, we observe a decrease of the Φ from 4.5 eV to 3.9 eV with the incorporation of CdS QDs onto the TiO_2 nanotubes.

Combining the optical band gap measurements and the UPS results, we can calculate the conduction band minimum (CB_m) for these samples [57]. CB_m energy levels of 0.74 and 0.64 eV with respect to the Fermi level were obtained for the $\text{NTs}_{\text{TiO}_2}$ and $\text{NTs}_{\text{TiO}_2} + \text{CdS}_{10\text{mM}-120 \text{ min}}$ samples,

respectively. These results are summarized in an apparent energy level diagram for the samples shown in figure 12. The values are plotted with respect to absolute scale (vacuum level in 0 eV) and the theoretical flat band potential for TiO_2 and CdS systems [50] are also shown in the center to gain a perspective for comparison.

In the case of the $\text{NTs}_{\text{TiO}_2}$ the band positions are very similar to the theoretical values of TiO_2 , showing that the UPS measurements combined with optical band gap techniques are robust for the determination of absolute band position of semiconductors. The band positions for the $\text{NTs}_{\text{TiO}_2} + \text{CdS}_{10\text{mM}-120 \text{ min}}$ sample are more similar to the theoretical values of CdS. Even when the estimated band positions for $\text{NTs}_{\text{TiO}_2} + \text{CdS}_{10\text{mM}-120 \text{ min}}$ are an average for band positions of TiO_2 and CdS semiconductors, a shift of the VB_M and CB_m to a more negative value for the TiO_2/CdS coupled systems if compared with only TiO_2 seems consistent. This result proves a strong contribution of CdS to the band positions on the surface in the sensitized samples, allowing electron transfer from the CdS nanoparticles to the TiO_2 NT semiconductors [56, 57].

In the case of the $\text{NTs}_{\text{TiO}_2} + \text{CdS}_{10\text{mM}-120 \text{ min}}$ sample, the electron separation is energetically ($\Phi = 3.9$ eV) more favorable than that of the TiO_2 NT material ($\Phi = 4.5$ eV); consequently, a more efficient charge separation (diminishing recombination) is achieved [58]. The more efficient charge separation combined with better absorption properties and inter-particle electron transfer in the sensitized samples leads to better photocatalytic activity for the water splitting reaction, as shown in this paper.

4. Conclusions

In summary, the sensitization via the *in situ* hydrothermal technique permits high loading and a uniform distribution of CdS quantum dots onto TiO_2 nanotubes. The behaviors of the different sizes and distribution of sizes of CdS QDs as a TiO_2 NT sensitizer for hydrogen production have been studied. As we increase the reaction time of CdS QD synthesis in the sensitized samples, the hydrogen production changes from not having an effect to inhibiting the hydrogen production and, finally, to improving the hydrogen production of the TiO_2 nanotube materials. The deactivation effect was related to two populations of sizes of CdS, where the population with a shorter band gap acts as a trap for the photogenerated electrons, diminishing the photocatalytic activity of TiO_2 in ultraviolet region. An improvement in the visible-light hydrogen generation rate ($0.3 \mu\text{mol cm}^{-2} \text{ h}^{-1}$) is achieved when sensitizing the TiO_2 NTs with CdS QDs (10 mM) obtained for 120 min of hydrothermal reaction. The good stability properties in the $\text{S}^{2-}/\text{SO}_3^{2-}$ sacrificial solution were achieved for long duration photocurrent experiments. The CdS stability against photocorrosion seems related to the nanotubular matrix and some protection inside the nanotubes as proved by the XPS depth profile in the case of air oxidation. The UPS studies confirm the electron transfer from CdS to TiO_2 and a more efficient charge separation in the

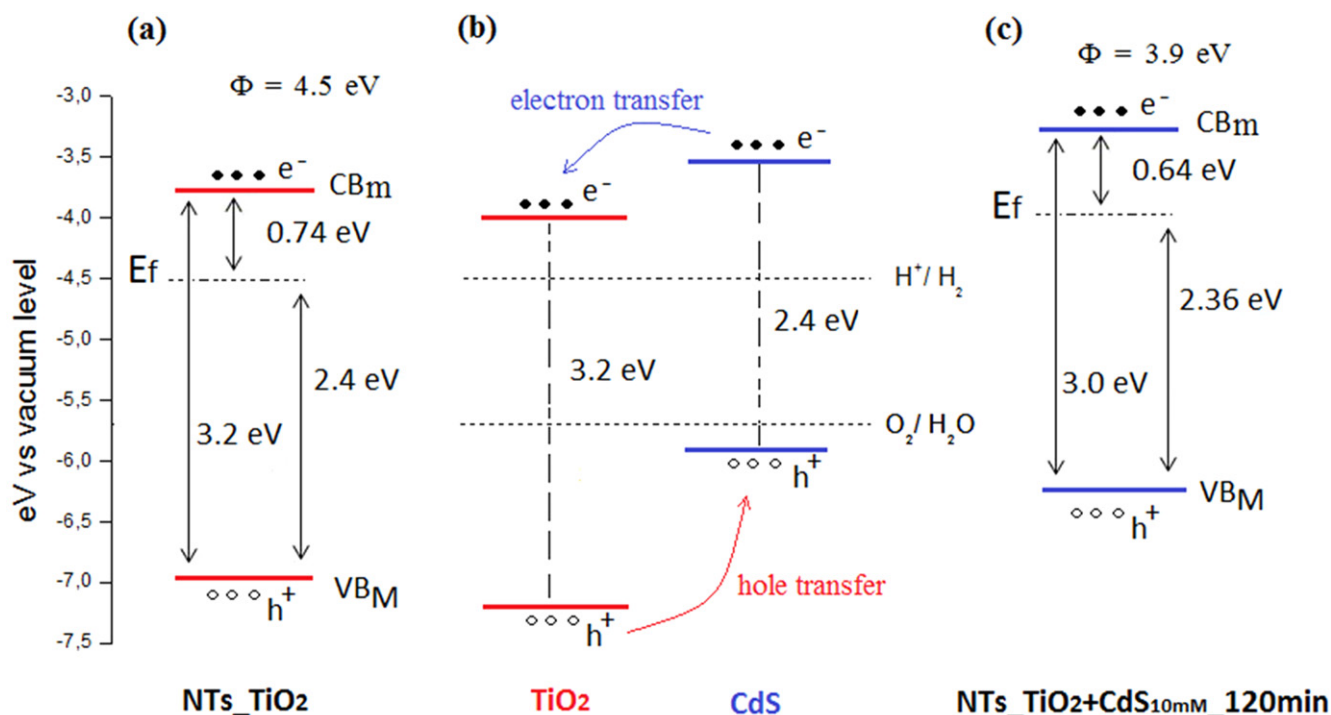


Figure 12. Schematic energy level diagrams with respect to absolute scale for NTs_TiO₂ (a) and NTs_TiO₂ + CdS_{10mM_120 min} (c). (Theoretic flat band potential for TiO₂ and CdS also is shown (b)).

sensitized samples. Both fundamental properties are related to the improvement of the visible-light hydrogen production for the TiO₂ NTs sensitized with CdS QDs. This paper highlights the possibility of using the *in situ* hydrothermal technique for the sensitization of TiO₂ NTs by CdS QDs for hydrogen production and also demonstrates that a UPS study combined with optical band gap measurements is a powerful tool for the characterization of coupled semiconductor systems.

Acknowledgments

This study was supported by CNPq, CAPES, FACEPE, CETENE, FINEP/CT-INFRA, and FAPERJ. CMA acknowledges support from Vatenkapsrådet (VR) and STandUP for Energy. AFS acknowledges support from the FAPESB/PRONEX/CNPq project.

References

- [1] Armor J N 1999 The multiple roles for catalysis in the production of H₂ *Appl. Catal. A* **176** 159–76
- [2] Fujishima A and Honda K 1972 Electrochemical photolysis of water at a semiconductor electrode *Nature* **238** 37–8
- [3] Chen X, Shen S, Guo L and Mao S S 2010 Semiconductor-based photocatalytic hydrogen generation *Chem. Rev.* **110** 6503–70
- [4] Paramasivam I, Jha H, Liu N and Schmuki P 2012 A review of photocatalysis using self-organized TiO₂ nanotubes and other ordered oxide nanostructures *Small* **8** 3073–103
- [5] Chen X and Mao S S 2007 Titanium dioxide nanomaterials: synthesis, properties, modifications, and applications *Chem. Rev.* **107** 2891–959
- [6] Fang D, Huang K, Liu S and Huang J 2008 Fabrication and photoluminescent properties of titanium oxide nanotube arrays *J. Braz. Chem. Soc.* **19** 1059–64
- [7] Cai Q, Paulose M, Varghese O K and Grimes C A 2011 The effect of electrolyte composition on the fabrication of self-organized titanium oxide nanotube arrays by anodic oxidation *J. Mater. Res.* **20** 230–6
- [8] Zhu K, Neale N R, Miedaner A and Frank A J 2007 Enhanced charge-collection efficiencies and light scattering in dye-sensitized solar cells using oriented TiO₂ nanotubes arrays *Nano Lett.* **7** 69–74
- [9] Ni M, Leung M K H, Leung D Y C and Sumathy K 2007 A review and recent developments in photocatalytic water-splitting using TiO₂ for hydrogen production *Renew. Sustain. Energy Rev.* **11** 401–25
- [10] Jun H K, Careem M A and Arof A K 2013 Quantum dot-sensitized solar cells—perspective and recent developments: a review of Cd chalcogenide quantum dots as sensitizers *Renew. Sustain. Energy Rev.* **22** 148–67
- [11] Emin S, Singh S P, Han L, Satoh N and Islam A 2011 Colloidal quantum dot solar cells *Sol. Energy* **85** 1264–82
- [12] Wang H, Luan C, Xu X, Kershaw S V and Rogach A L 2012 *In situ* versus *ex situ* assembly of aqueous-based thioacid capped CdSe nanocrystals within mesoporous TiO₂ films for quantum dot sensitized solar cells *J. Phys. Chem. C* **116** 484–9
- [13] Kim J C, Choi J, Lee Y B, Hong J H, Lee J I, Yang J W, Lee W I and Hur N H 2006 Enhanced photocatalytic activity in composites of TiO₂ nanotubes and CdS nanoparticles *Chem. Commun.* 5024–6
- [14] Ratanatawanate C, Xiong C and Balkus K J 2008 Fabrication of PbS quantum dot doped TiO₂ nanotubes *ACS Nano* **2** 1682–8

- [15] Zhou Q, Fu M-L, Yuan B-L, Cui H-J and Shi J-W 2011 Assembly, characterization, and photocatalytic activities of TiO₂ nanotubes/CdS quantum dots nanocomposites *J. Nanoparticle Res.* **13** 6661–72
- [16] Kontos A G, Likodimos V, Vassalou E, Kapogianni I, Raptis Y S, Raptis C and Falaras P 2011 Nanostructured titania films sensitized by quantum dot chalcogenides *Nanoscale Res. Lett.* **6** 266
- [17] Dibbell R S and Watson D F 2009 Distance-dependent electron transfer in tethered assemblies of CdS quantum dots and TiO₂ nanoparticles *J. Phys. Chem. C* **113** 3139–49
- [18] Qian S, Wang C, Liu W, Yinhua Zhu, Wenjun Y and Xiaohua L 2011 An enhanced CdS/TiO₂ photocatalyst with high stability and activity : effect of mesoporous substrate and bifunctional linking molecule *J. Mater. Chem.* **21** 4945–52
- [19] Sant P A and Kamat P V 2002 Interparticle electron transfer between size-quantized CdS and TiO₂ semiconductor nanoclusters Dedicated to Professor Frank Wilkinson on the occasion of his retirement *Phys. Chem. Chem. Phys.* **4** 198–203
- [20] Robel I, Kuno M and Kamat P V 2007 Size-dependent electron injection from excited CdSe quantum dots into TiO₂ nanoparticles *J. Am. Chem. Soc. Commun.* **129** 4136–7
- [21] Grimes C A and Mor G K 2009 *TiO₂ Nanotube Arrays* (Boston, MA: Springer US) ch 2 pp 67–114
- [22] Song X, Wang M, Shi Y, Deng J, Yang Z and Yao X 2012 *In situ* hydrothermal growth of CdSe(S) nanocrystals on mesoporous TiO₂ films for quantum dot-sensitized solar cells *Electrochim. Acta* **81** 260–7
- [23] Macak J M, Tsuchiya H, Ghicov A, Yasuda K, Hahn R, Bauer S and Schmuki P 2007 TiO₂ nanotubes: self-organized electrochemical formation, properties and applications *Curr. Opin. Solid State Mater. Sci.* **11** 3–18
- [24] Kraeutler B and Bard A J 1978 Heterogeneous photocatalytic decomposition of saturated carboxylic acids on TiO₂ powder. Decarboxylative route to alkanes *J. Am. Chem. Soc.* **100** 5985–92
- [25] Chong S V, Suresh N, Xia J, Al-salim N and Idriss H 2007 TiO₂ nanobelts/CdSSe quantum dots nanocomposite *J. Phys. Chem. C* **111** 10389–93
- [26] Gonbeau D, Guimon C, Pfister-Guillouzo G, Levasseur A, Meunier G and Dormoy R 1991 XPS study of thin films of titanium oxysulfides *Surf. Sci.* **254** 81–9
- [27] Regonini D, Jaroenworarluck A, Stevens R and Bowen C R 2010 Effect of heat treatment on the properties and structure of TiO₂ nanotubes: phase composition and chemical composition *Surf. Interface Anal.* **42** 139–44
- [28] Zhang W, Cao L, Wan L, Liu L and Xu F 2013 A photoelectron spectroscopy study on the interfacial chemistry and electronic structure of terephthalic acid adsorption on TiO₂ (110)-(1 × 1) surface *J. Phys. Chem. C* **117** 21351–8
- [29] Pan D, Wang Q, Pang J, Jiang S, Ji X and An L 2006 Semiconductor ‘nano-onions’ with multifold alternating CdS/CdSe or CdSe/CdS structure *Chem. Mater.* **18** 4253–8
- [30] Chaguetmi S, Mammeri F, Pasut M, Nowak S, Lecoq H, Decorse P, Costentin C, Achour S and Ammar S 2013 Synergetic effect of CdS quantum dots and TiO₂ nanofibers for photoelectrochemical hydrogen generation *J. Nanoparticle Res.* **15** 2140
- [31] Li H, Shih W Y and Shih W-H 2007 Synthesis and characterization of aqueous carboxyl-capped CdS quantum dots for bioapplications *Ind. Eng. Chem. Res.* **46** 2013–9
- [32] Robel I, Subramanian V, Kuno M and Kamat P V 2006 Quantum dot solar cells. harvesting light energy with CdSe nanocrystals molecularly linked to mesoscopic TiO₂ films *J. Am. Chem. Soc.* **128** 2385–93
- [33] Jeong K S *et al* 2012 Enhanced mobility-lifetime products in PbS colloidal quantum dot photovoltaics *ACS Nano* **6** 89–99
- [34] Nagaoka H, Colbert A E, Strein E, Janke E M, Salvador M, Schlenker C W and Ginger D S 2014 Size-dependent charge transfer yields in conjugated polymer/quantum dot blends *J. Phys. Chem. C* **118** 5710–5
- [35] Alivisatos A P 1996 Perspectives on the physical chemistry of semiconductor nanocrystals *J. Phys. Chem.* **100** 13226–39
- [36] Brus L E 1984 Electron–electron and electron-hole interactions in small semiconductor crystallites: the size dependence of the lowest excited electronic state *J. Chem. Phys.* **80** 4403
- [37] Winter J O, Gomez N, Gatzert S, Schmidt C E and Korgel B A 2005 Variation of cadmium sulfide nanoparticle size and photoluminescence intensity with altered aqueous synthesis conditions *Colloids Surfaces A* **254** 147–57
- [38] Guo J, Yang W and Wang C 2005 Systematic study of the photoluminescence dependence of thiol-capped CdTe nanocrystals on the reaction conditions *J. Phys. Chem. B* **109** 17467–73
- [39] Yu W W, Qu L, Guo W and Peng X 2003 Experimental determination of the extinction coefficient of CdTe, CdSe, and CdS nanocrystals *Chem. Mater.* **15** 2854–60
- [40] Vossmeier T, Katsikas L, Gienig M, Popovic I G, Diesner K, Chemseddine A, Eychmüller A and Weller H 1994 CdS nanoclusters : synthesis, characterization, size dependent oscillator strength, temperature shift of the excitonic transition energy, and reversible absorbance shift *J. Phys. Chem.* **98** 7665–73
- [41] Tauc J and Menth A 1972 States in the gap *J. Non. Cryst. Solids* **8-10** 569–85
- [42] Kisch H 2013 Semiconductor photocatalysis—mechanistic and synthetic aspects *Angew. Chem., Int. Ed. Engl.* **52** 812–47
- [43] Reddy K M, Manorama S V and Reddy A R 2002 Bandgap studies on anatase titanium dioxide nanoparticles *Mater. Chem. Phys.* **78** 239–45
- [44] Gui-Sheng L, Die-Qing Z and Jimmy C Y 2009 A new visible-light photocatalyst : CdS quantum dots embedded *Environ. Sci. Technol.* **43** 7079–85
- [45] Gomathisankar P, Hachisuka K, Katsumata H, Suzuki T, Funasaka K and Kaneco S 2013 Photocatalytic hydrogen production from aqueous Na₂S + Na₂SO₃ solution with B-doped ZnO *ACS Sustain. Chem. Eng.* **1** 982–8
- [46] Li Q, Guo B, Yu J, Ran J, Zhang B, Yan H and Gong J R 2011 Highly efficient visible-light-driven photocatalytic hydrogen production of CdS-cluster-decorated graphene nanosheets *J. Am. Chem. Soc.* **133** 10878–84
- [47] Gao C, Zhang Z, Li X, Chen L, Wang Y, He Y, Teng F, Zhou J, Han W and Xie E 2015 Synergistic effects in three-dimensional SnO₂/TiO₂/CdS multi-heterojunction structure for highly efficient photoelectrochemical hydrogen production *Sol. Energy Mater. Sol. Cells* **141** 101–7
- [48] Li C, Yuan J, Han B, Jiang L and Shangguan W 2010 TiO₂ nanotubes incorporated with CdS for photocatalytic hydrogen production from splitting water under visible light irradiation *Int. J. Hydrogen Energy* **35** 7073–9
- [49] Yaojun Z, Yanpei W, Zhenhua W and Yaru H 2009 Preparation of CdS/TiO₂NTs nanocomposite and its activity of photocatalytic hydrogen production *Rare Met. Mater. Eng.* **38** 1514–7
- [50] Bessekhoud Y, Robert D and Weber J 2004 Bi₂S₃/TiO₂ and CdS/TiO₂ heterojunctions as an available configuration for photocatalytic degradation of organic pollutant *J. Photochem. Photobiol. A* **163** 569–80
- [51] Kongkanand A, Tvrđy K, Takechi K, Kuno M, Kamat P V and Dame N 2008 Quantum dot solar cells. Tuning photoresponse through size and shape control of CdSe—TiO₂ architecture *J. Am. Chem. Soc.* **130** 4007–15

- [52] Osada N, Oshima T, Kuwahara S, Toyoda T, Shen Q and Katayama K 2014 Photoexcited carrier dynamics of double-layered CdS/CdSe quantum dot sensitized solar cells measured by heterodyne transient grating and transient absorption methods *Phys. Chem. Chem. Phys.* **16** 5774–8
- [53] Pareek A, Purbia R, Paik P, Hebalkar N Y, Kim H G and Borse P H 2014 Stabilizing effect in nano-titania functionalized CdS photoanode for sustained hydrogen generation *Int. J. Hydrogen Energy* **39** 4170–80
- [54] Seabold J A and Neale N R 2015 All first row transition metal oxide photoanode for water splitting based on Cu₃V₂O₈ *Chem. Mater.* **27** 1005–13
- [55] Hisatomi T, Kubota J and Domen K 2014 Recent advances in semiconductors for photocatalytic and photoelectrochemical water splitting *Chem. Soc. Rev.* **43** 7520–35
- [56] Peng R, Lin C, Baltrusaitis J, Wu C-M, Dimitrijevic N M, Rajh T, May S and Koodali R T 2014 Insight into band positions and inter-particle electron transfer dynamics between CdS nanoclusters and spatially isolated TiO₂ dispersed in cubic MCM-48 mesoporous materials: a highly efficient system for photocatalytic hydrogen evolution *Phys. Chem. Chem. Phys.* **16** 2048–61
- [57] Liu G, Jaegermann W, He J, Sundstro V and Sun L 2002 XPS and UPS characterization of the TiO₂/ZnPcGly heterointerface: alignment of energy levels *J. Phys. Chem. B* **106** 5814–9
- [58] Wang G, Wang H, Ling Y, Tang Y, Yang X, Fitzmorris R C, Wang C, Zhang J Z and Li Y 2011 Hydrogen-treated TiO₂ nanowire arrays for photoelectrochemical water splitting *Nano Lett.* **11** 3026–33